P3.25 NOCTURNAL TORNADOES AND LOW-LEVEL STATIC STABILITY

Amanda K. Kis*,, Jerry M. Straka* and Katharine M. Kanak***
***University of Oklahoma, Norman, Oklahoma**
****Storm Prediction Center**

1. INTRODUCTION

Nocturnal tornadoes, while comprising only about a quarter of verified tornadoes, produce 42.5 percent of tornado fatalities (Ashley 2007). However, very little investigation into the dynamics unique to nocturnal tornadoes exists in the literature. It seems likely that changes over the diurnal cycle would change the dynamics between daytime and nighttime tornadoes. For example, the nature of inflow might vary as the daytime boundary layer transitions into the nocturnal stable boundary layer. Also, storm type at night may skew away from the archetypal "isolated" supercell to other modes.

The first part of the following study examines a climatology of significant (F2 and greater) nocturnal tornadoes. The climatology includes spatial and temporal data, radar observations of storm mode, and proximity soundings.

The second part of the study numerically models an idealized supercell in which descending precipitation triggers tornadogenesis. Static stability tability of the lowest kilometer is varied to approximate shallow nocturnal boundary layers of varying stability and test their effects on tornadogenesis.

2. CLIMATOLOGY

2.1 Methodology

Official National Weather Service (NWS) Storm Data reports obtained through the SVRPLOT software (Hart 1993) were used to construct a climatology of significant nocturnal tornadoes occurring in the contiguous United States between January 1, 2004 and December 31, 2006. Per previous climatologies (e.g. Guyer et al. 2006), nocturnal tornadoes were defined as those occurring between 03 UTC – 13 UTC. The climatology was restricted to significant tornadoes in an effort to eliminate non-supercellular cases and enable focus on the diurnally varying dynamics of tornadogenesis unique to supercell thunderstorms. Tropical events were removed. These criteria produced a sample of 69 tornadoes (Table 1).

Weather Surveillance Radar-1988 Doppler (WSR-88D) NEXRAD reflectivity data from the National Climatic Data Center (NCDC) online archive was available for 66 cases. Storm mode was analyzed and categorized for these cases (Table 1). The six resulting categories were: Supercell embedded in a continuous squall line (Fig. 1a); broken line of supercells (Fig. 1b); and supercell on the southern end of a squall line (Fig. 1c). The other categories were: Isolated supercell (Fig. 1d); supercell embedded in a multicell cluster (Fig. 1e); and supercell embedded in the leading edge of a mesoscale convective system (MCS) (Fig. 1f).

Given the sparse coverage of observed soundings, Rapid Update Cycle-2 (RUC-2) model proximity soundings were used to approximate environmental conditions in the inflow regions of tornadoes on our sample. RUC-2 analysis gridpoint soundings were generated hourly for each tornado in the climatology. Those immediately before and after each event were gathered and viewed using the NSHARP software (Hart and Korotky 1991). Spatial proximity of 80 km was required, and soundings were taken upwind from the tornadoes in an area assumed to characterize the inflow region (i.e. between 90 and 180 degrees). These criteria identified at least one proximity sounding for 28 of the events (Table 2).

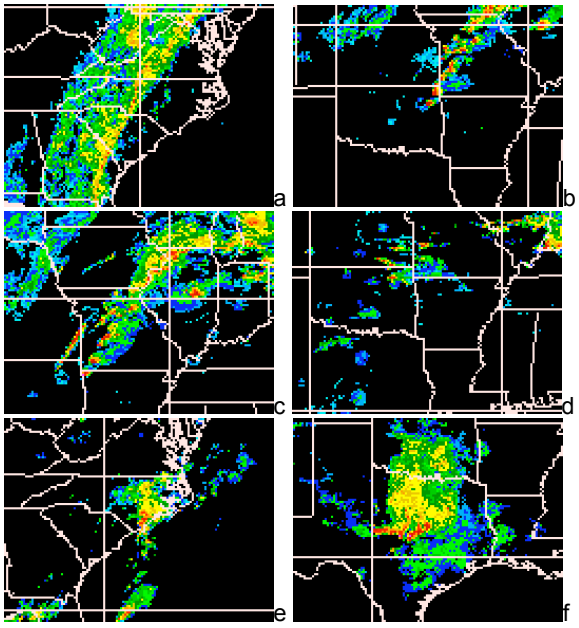

Fig. 1: Examples of Dopper radar reflectivity for: Supercell embedded in a continuous line (a); broken line of supercells (b); supercell on the southern end of a squall line (c); isolated cell (d); multicell cluster (e); and supercell on southern edge of MCS (f).

2.2 Results

All of the cases identified in the climatology occurred east of the Rocky Mountains. Thirty-eight tornadoes—eighteen in Gulf Coast states—occurred during the cool season (defined herein as October 15 – February 15). Guyer et al. (2006) gathered a similar 20-year climatology of cool season significant tornadoes in the Gulf Coast states and found a large

Corresponding author address: Amanda K. Kis, University of Oklahoma, School of Meteorology Norman, OK 73072; e-mail: akkis@ou.edu

Date (mm/dd/yyyy)	Time (UTC)	Latitude (degrees)	Longitude (degrees)	State	Strength	Storm Mode
01/25/2004	1246	30.15	92.1	LA	F2	Southern end
05/25/2004	434	39.72	90.27	IL	F2	Continous line
05/27/2004	319	37.97	93.95	MO	F2	Isolated
05/30/2004	330	39.88	94.25	MO	F4	Isolated
05/30/2004	417	35.83	96.6	OK	F3	Isolated
08/13/2004	754	34.4	77.88	NC	F2	MCS
11/24/2004	539	31.72	91.2	MS	F3	Southern end
11/24/2004	400	31.17	94.88	TX	F2	Continuous line
11/24/2004	654	31.75	90.12	MS	F2	Multicell
11/24/2004	715	32.6	89.75	MS	F2	Multicell
11/24/2004	630	30.3	89.85	LA	F2	Isolated
11/24/2004	752	32.02	89.53	MS	F2	Broken line
11/24/2004	824	32.92	89	MS	F3	Broken line
11/24/2004	1009	32.17	37.73	AL	F2	Continous line
11/24/2004	1148	32.6	86.9	AL	F2	Continuous line
11/24/2004	1200	30.43	89.08	MS	F2	Continuous line
11/24/2004	1224	32.38	86.67	AL	F2	Continuous line
11/24/2004	1258	33.58	86.07	AL	F2	Continuous line
12/07/2004	719	32.13	90.92	MS	F2	Continuous line
12/07/2004	813	34.07	89	MS	F2	Continuous line
12/07/2004	954	33.53	88.35	MS	F2	Continuous line
12/10/2004	949	33.57	80.83	SC	F3	Continuous line
12/10/2004	1000	33.65	80.78	SC	F2	Continuous line
01/08/2005	334	31.18	89.4	MS	F2	Continous line
01/13/2005	458	32.73	93.13	LA	F2	Isolated
01/13/2005	525	33.02	92.73	AR	F3	Multicell
01/14/2005	645	35.57	80.38	NC	F2	Continuous line
04/06/2005	1210	32.13	90.12	MS	F3	Southern end
04/06/2005	1249	31.05	90.33	MS	F2	Continuous line
11/06/2005	419	36.52	91.38	MO	F2	Continuous line
11/06/2005	438	36.55	91.15	AR	F2	Continuous line
11/06/2005	739	37.83	87.78	KY	F3	Continuous line
11/06/2005	746	37.42	88.05	KY	F3	Continuous line
11/06/2005	1040	37.28	85.92	KY	F2	Continuous line
11/28/2005	430	36.53	91.1	MO	F2	N/A
01/13/2006	428	35.12	93.35	AR	F2	Continuous line
02/02/2006	839	29.98	90.15	LA	F2	MCS
03/09/2006	1249	35.2	91.15	AR	F2	Broken line
03/12/2006	319	37.82	90	MO	F3	Isolated
03/12/2006	342	38.12	90.33	MO	F3	Broken line
03/13/2006	300	39.93	89.28	IL	F2	Broken line
03/13/2006	308	36.1	95.1	OK	F3	Southern end
03/13/2006	317	39.32	92.48	MO	F3	Broken line
03/13/2006	337	36.23	94.65	OK	F3	Southern end
03/13/2006	343	39.45	92.18	MO	F4	Broken line
03/13/2006	410	36.35	94.23	AR	F2	Southern end
03/13/2006	415	36.98	93.8	MO	F3	Broken line
03/13/2006	416	37.85	93.43	MO	F3	Broken line
03/13/2006	419	38.28	92.85	MO	F2	Broken line
03/13/2006	502	37.2	93	MO	F2	Broken line
03/13/2006	515	37.25	92.87	MO	F3	Broken line

03/13/2006	600	38.85	91.32	MO	F3	Isolated
03/13/2006	630	38.77	92.07	MO	F2	Continuous line
03/13/2006	719	39.05	91.37	MO	F3	Continuous Line
03/20/2006	419	29.22	99.72	TX	F2	Isolated
04/03/2006	325	35.6	89.3	TN	F2	Broken line
04/08/2006	730	34.02	85.07	GA	F2	Continuous line
04/14/2006	307	41.27	90.62	IL	F2	MCS
04/29/2006	1234	30.6	95.15	TX	F2	Continuous line
05/06/2006	545	31.55	97.15	TX	F2	MCS
05/10/2006	337	33.37	96.52	TX	F3	Southern end
10/17/2006	839	31.5	89.57	MS	F2	N/A
11/15/2006	755	31.25	90.9	LA	F2	Broken line
11/15/2006	830	31.58	90.05	MS	F3	Broken line
11/15/2006	849	31.62	90.58	LA	F2	Broken line
11/15/2006	931	32.03	89.13	MS	F3	Continuous line
11/16/2006	422	35.88	81.13	NC	F2	N/A
11/16/2006	1137	34.57	78.4	NC	F3	MCS

Table 1: Cases defined by climatology. Storm mode is abbreviated for: Supercell embedded within continuous line of storms ("Continuous line"); broken line of supercells ("Broken line"); supercell on southern end of line of storms ("Southern end"); isolated supercell ("Isolated"); multicell cluster ("Multicell"); and leading edge of MCS ("MCS"). "N/A" means that radar data was not available.

Date (mm/dd/yyyy)	Time (UTC)	Station I.D.	Distance (mi)	Station I.D.	Distance (mi)
05/30/2004	330	P#I	17		
11/24/2004	400	KLFK	5		
11/24/2004	654	CLN	34	KPIB	48
11/24/2004	715	CLN	66		
11/24/2004	752	CLN	22	KPIB	37
11/24/2004	715	KMGM	33		
11/24/2004	1224	KMGM	15		
01/08/2005	334	KGPT	41		
11/06/2005	419	KJBR	57		
11/06/2005	438	KJBR	51		
11/06/2005	440	KJBR	45		
11/06/2005	746	KBWG	79		
01/13/2006	428	KHOT	43	RUE	16
03/13/2006	308	KFYV	48		
03/13/2006	337	KFYV	28		
03/13/2006	410	KFYV	18		
03/13/2006	415	UMN	4		
03/13/2006	416	KSGF	43	P#H	39
03/13/2006	419	P#H	48		
03/13/2006	600	KSUS	31		
03/13/2006	630	KSUS	65		
03/13/2006	719	KSUS	38		
04/08/2006	730	KFTY	29		
05/06/2006	545	KACT	1		
10/17/2006	839	KPIB	17		
11/15/2006	849	KMCB	29		
11/16/2006	422	KCLT	37		
11/16/2006	1137	ILM	36	KILM	28

Table 2: RUC-2 proximity sounding data for those cases that fit the criteria. "Distance" is the distance between the tornado and the proximity soundings.

portion of the sample occurred overnight. Fike (1993) noted a similar maximum. Thirty tornadoes occurred during spring and reflected the seasonal shift of severe weather into the southern and central Plains states. These geographic maximums are reflected in the denser clusters of tornadoes in Figure 2.

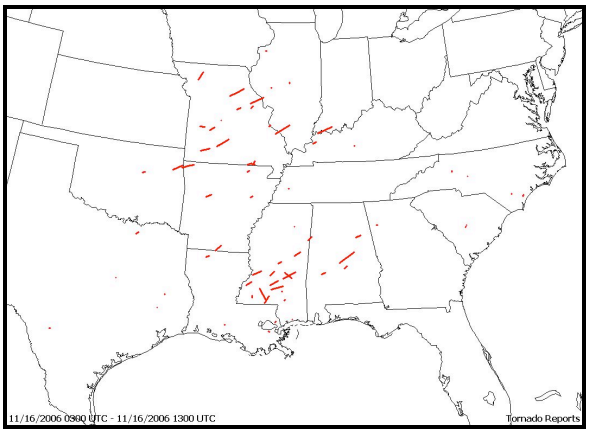

Fig. 2: Track for each tornado in the sample, produced with Severe Plot software.

Tornado activity trended rapidly downward after an initial late afternoon maximum. This downward trend coincides with increased radiational cooling. A secondary maximum occurred between 07 UTC – 08 UTC, with the downward trend continuing afterwards. Activity increased at 13 UTC as solar insolation increased.

Forty-eight tornadoes occurred in squall lines. Of these cases, twenty-seven occurred in supercells embedded within a continuous squall line, twelve occurred in a broken line of supercells, and seven occurred in a supercell on the southern end of a squall line. These modes were dominant during the cool season. Only seven tornadoes occurred with in isolated supercells. These mainly occurred during the spring. Of the remaining eight cases, seven occurred in supercells embedded in multicellular clusters and one occurred in a supercell embedded in the leading edge of an MCS. While tornadoes are classically attributed to isolated supercells, Trapp et al. (2004) found that quasi-linear systems (QLCS) accounted for significantly more cool season tornadoes than did isolated cells. Also, more nocturnal tornadoes occurred in QLCS, with a higher percentage of significant tornadoes than weak tornadoes.

Of the 28 cases with appropriate model proximity soundings, RUC-2 proximity soundings indicated sixteen cases with stable boundary layers in at least one surrounding sounding. Of these sixteen cases, the stable layer occurred only in the sounding after the tornado in eight cases; in the other eight, a stable layer was present at least in the sounding before the tornado. The depths varied from a minimum of 84.0 m to a maximum of 481.9 m, with an average depth of 303.24 m.

3. NUMERICAL MODEL SIMULATION

3.1 Background

The dynamic pipe effect (DPE) (Leslie 1971) is a hypothesis that tornadoes are downward-building extensions of the mid-level mesocyclone characteristic of parent supercells. The mid-level mesocyclone builds downward as the rotating updraft ingests ambient air and establishes cyclostrophic balance progressively lower. Because the mesocyclone is in cyclostrophic balance, air cannot enter through its lateral boundary. Instead, air must be drawn upwards by the updraft from below the mesocyclone. Thus, the lowering mesocyclone acts as a solid "pipe," drawing air through the bottom opening of the pipe. Eventually, this process works down to the ground and results in a tornado.

Leslie and Smith (1978) (hereafter LS78) investigated the effects of low-level stability on the DPE. Using an axisymmetric model, they modeled a tornado-like vortex and varied the stability of the lowest kilometer. Vertical motion and radial convergence decreased as static stability increased. The vortices ingested potentially cold air from the stable layer, which decreased their buoyancy and weakened them further. These effects resulted in wider and weaker vortices, some of which terminated aloft.

Davies-Jones (2008) hypothesized and demonstrated numerically a mode of tornadogenesis independent of the DPE. In this mechanism, a descending rain curtain instigates tornadogenesis by concentrating barotropic vorticity into a tornado. Rain descends from the top of the storm along the updraft-downdraft interface in an annular, precipitation-driven downdraft. This descending rain curtain drags air with high angular momentum to the surface. This increases tangential acceleration and creates positive vertical vorticity next to the surface. Then, upward recycling of precipitation-laden air by the low-level updraft amplifies the vertical vorticity through stretching and eventually producing tornadogenesis.

We will closely reproduce Davies-Jones's (2008) simulation in a three-dimensional model, and vary the stability of the lowest kilometer in order to examine the effects of low-level static stability on tornadogenesis independent of the DPE.

3.2 Numerical Model Description

Straka's Atmospheric Model (SAM) is a three-dimensional, fully compressible, non-hydrostatic model. For this study, SAM is employed with the incompressible Navier-Stokes equations. A quadratic conserving, second-order centered-in-space "box" finite difference scheme is used for scalars and velocities. A centered-in-time Leapfrog finite difference scheme is used for temporal integration. A sixth-order numerical filter and divergent damping are also applied. The model is run using MPI on a massively parallel architecture.

3.3 Experimental Design

3.3.1 Domain Parameters

The non-rotating domain is 20 km x 20 km x 12.2 km, with both horizontal and vertical grid spacing of 100 m. This domain is sufficiently large to model both the parent supercell and tornado.

The lateral boundaries are open as in Klemp and Wilhelmson (1978) but with no intrinsic gravity wave velocity for outflow (dry adiabatic sounding). Lewellen and Lewellen (2007) note that an open domain may be dangerous if the simulated storm becomes so strong as to force unknown feedbacks outside the domain. However, since the downdraft is entirely within the domain, inflow does not enter through the lateral boundaries. The upper boundary is closed and rigid. The lower boundary is impermeable, free-slip, and rigid. Fick's first law is invoked for diffusion and is used for the sub-grid turbulence closure scheme, with a mixing coefficient of K = 100 m^2 s^{-1}.

3.3.2 Initial Condition

The thermodynamic base state profile is dry neutral, with θ_0 = 300 K. Density is held constant at 1 g kg^{-1} throughout the domain. With these conditions, no baroclinic vorticity can be produced.

The initial flow is Beltrami, and approximates a steady, mature supercell with cyclonically rotating updraft (with rotation maximized at mid-levels) surrounded by an anticyclonically rotating downdraft. The equations governing the initial Beltrami flow are detailed in Section III of Davies-Jones (2008), cast here in Cartesian coordinates and with the decay term neglected. The velocity fields are prescribed according to the following equations:

$$u_o = -(\mu / k) W_o J_1(k\sqrt{x^2 + y^2}) \cos(\mu z) \qquad (1)$$

$$v_o = (\lambda / k) W_o J_1(k\sqrt{x^2 + y^2}) \sin(\mu z) \qquad (2)$$

$$w_o = W_o J_o(k\sqrt{x^2 + y^2}) \sin(\mu z) \qquad (3)$$

where W_0 is the initial maximum upward velocity. The value of W_0 also serves as the thermodynamic speed limit (Fiedler and Rotunno 1986). These equations describe a helical flow, where u, v, and w are the three-dimensional wind components, x, y, and z are the three Cartesian directions, λ is the constant rate at which the wind veers with height, μ is π/L_z, k = $(\lambda^2 - \mu^2)^{(1/2)}$, J_0 is the Bessel function of zero order (six terms retained), and J_1 is the Bessel function of first-order (six terms retained).

Initial amplitudes of u $_0$, v $_0$, w $_0$, perturbation vertical vorticity (ζ'_0), and perturbation pressure (p'_0) are specified in Table 3. The resulting initial flow is pictured in Fig. 3. This initial flow is slightly off-center, which results in slight storm tilt with height as the simulations progress.

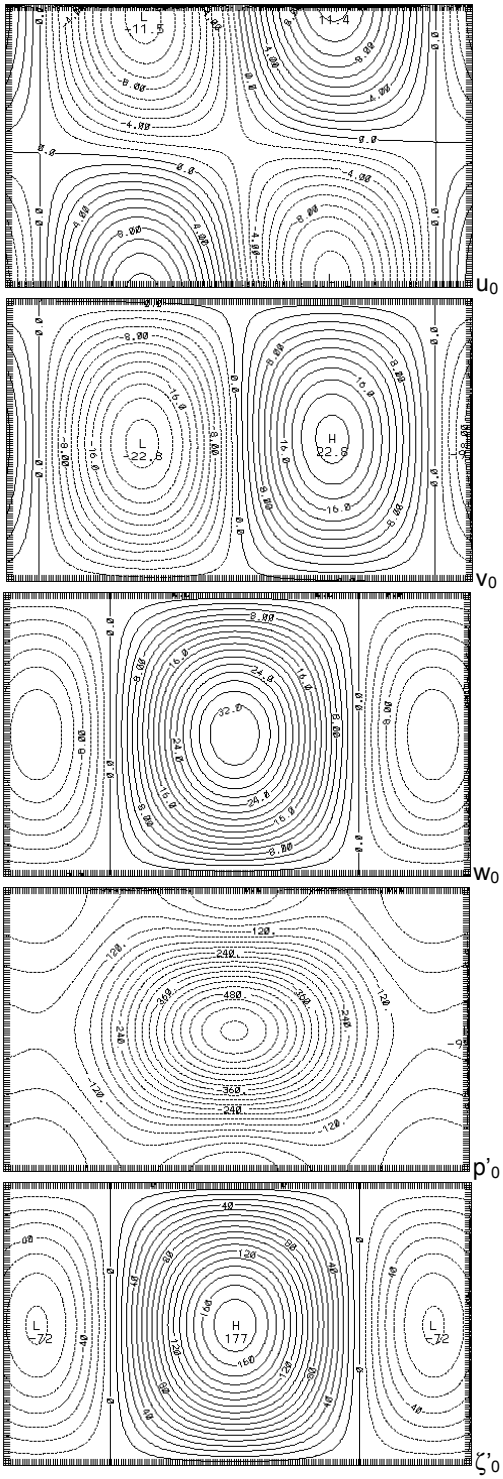

Fig. 3: Initial Beltrami flow. (Units of u_0, v_0, and w_0 are m s^{-1}. Units of p'_0 are Pa. Units of ζ_0 are s^{-1}. The inteval Δu_0 = 1 m s^{-1}; Δv_0 = 2 m s^{-1}; Δw_0 = 2 m s^{-1}; $\Delta p'_0$ = 30 Pa; and $\Delta \zeta'_0$ = 10 x 10^{-3} s^{-1}.)

As there is no body force / latent heat release, and no continuous updraft is defined (as in Lewellen et al. 1997) only tornadogenesis is simulated. Upon

tornadogenesis, the downward directed pressure gradient force drives a downdraft down the center of the axial updraft, and results in the dissipation of the tornado owing to the lack of a continuously forced updraft. Thus, tornado maintenance and decay are not simulated.

Max{u_0}	Min{u_0}	Max{v_0}	Min{v_0}
22.8	-22.8	22.8	-22.8
Max{w_0}	Min{w_0}	Max{ζ'_0}	Min{ζ'_0}
34.0	-13.7	1.78×10^{-2}	-7.2×10^{-3}

Table 3: Initial amplitudes of Beltrami flow. (Units of u_0, v_0, and w_0 are m s^{-1}. Units of ζ'_0 are s^{-1}. Units of θ_0 are K.)

Hydrometeors are characterized by liquid water only (i.e. they are characterized by a fall speed and drag only). Drops are assumed to be large (a few mm in diameter) and fall quickly (about 8.5 m s^{-1}) so that evaporation is minimal and can be assumed to be negligible. Hydrometeors are released at the first time-step and thereafter. The rain mixing ratio, q, is specified as circular disc atop the cyclonic circulation. It is maximized, with a value of q_{max}. It then varies outward as:

$$q(x,y,z_{top},t) = q_{\max} J_o\left(k\sqrt{x^2+y^2}\right) \times\left[1-\exp\left(-t^2/\tau^2\right)\right] \quad (4)$$

where r is radius, r<(2.4048)/k, and $\tau = 0.5\ L_z/W_o$.

Starting at the first time step, the initial thermodynamic profile is relaxed in the lowest kilometer to a specified profile representing a shallow stable layer. Flow above one kilometer, representing the parent supercell, is constrained to "float" above the stable layer—that is, momentum from the stable layer can be drawn into the supercell but colder temperatures cannot.

3.3.3 Control Run and Suite of Experiments

The control run (CR) sets q_{max} = 5 g kg^{-1} (Fig. 4a). It is run for 3000 s. The results of CR are used for comparison and analysis with the other experiments.

	θ_s (K)	Lapse rate in lowest kilometer (_ km^{-1})
CR	300	0
ST2	298	2
ST3	297	3
ST4	296	4
ST5	296	5

Table 4: Experimental design. θ_s is the surface potential temperature.

Experiments 1 – 4 (ST2, ST3, ST4, and ST5) are summarized in Table 4. These are also run for 3000 s. In each experiment, the temperature profile in the lowest kilometer is relaxed to a surface temperature θ_s, $\theta_s < \theta_0$. The one-kilometer stable layers produced in the experiments approximate shallow nocturnal boundary layers with varying degrees of stability. Values of θ_s can be compared to Table 1 in LS78.

3.4 Results

Davies-Jones (2008) defined a mesocyclone as a cyclonic vortex with core radius greater than two kilometers, a tornado cyclone (TC) as a cyclonic vortex with core radius less than two kilometers that does not break the thermodynamic speed limit, and a tornado as a cyclonic vortex with core radius less than two kilometers that does break the thermodynamic speed limit. These same definitions will be used in this study. This study also defines an incipient tornado as a cyclonic vortex with core radius less than two kilometers, which forms within the TC and evolves directly into the tornado.

3.4.1 Control run

After their release, the hydrometeors diverge away at the top of the updraft, and descend as a precipitation-driven annular rain curtain through the updraft-downdraft interface. As the rain curtain descends, it is advected cyclonically around the rotating updraft, creating a "twisting" downdraft (Fujita 1973). The rain curtain passes through air with high angular momentum, and drags this air towards the surface. Inflow causes the rain curtain to curve slightly inwards beneath the mid-level mesocyclone as it descends. The rain curtain reaches the ground at about 1080 s and converges inward due to both mass conservation and radial inflow. Cyclonic flow is maintained as hydrometeors converge towards the low-level updraft.

As the rain curtain reaches the ground, the air enters the updraft. Angular momentum is drawn inwards, increasing tangential acceleration beneath the mid-level mesocyclone and producing positive vertical vorticity. The air is recycled upwards by the updraft, which amplifies the positive vertical vorticity through stretching. Consequently, the mid-level mesocyclone spins-up slightly (~ 3.5 x 10-2 s^{-1}).

Establishment of cyclostrophic balance is attempted as tangential acceleration increases within the updraft below mid levels. Pressure accordingly decreases, driving a stronger radial component of the flow. This draws more high angular momentum air into the updraft, enhancing the process and increasing rotation below mid levels. As convergence of angular momentum beneath the mid-level mesocyclone continues, a TC develops at about 1860 s as a downward extension of the mid-level mesocyclone (4a).

At about 2160 s, an incipient tornado develops independently of the mid-level mesocyclone and TC.

The incipient tornado develops at about 1.5 km above the surface as convergence and recycling of the high angular momentum air are maximized at and just above the surface (Fig. 4b). It lowers towards the surface and contracts into a tornado at about 2310 s (Fig 4c). Its maximum strength is reached between 2460 s and 2490 s (Fig. 4d), and is characterized by intense upward motion of 131.7 m s^{-1} (nearly four times stronger than the thermodynamic speed limit), ζ' of 1.37 s^{-1}, radial inflow over 100 m s^{-1}, and a pressure deficit of 11216.5 Pa (nearly 20 times larger than the initial deficit in the mid-level mesocyclone).

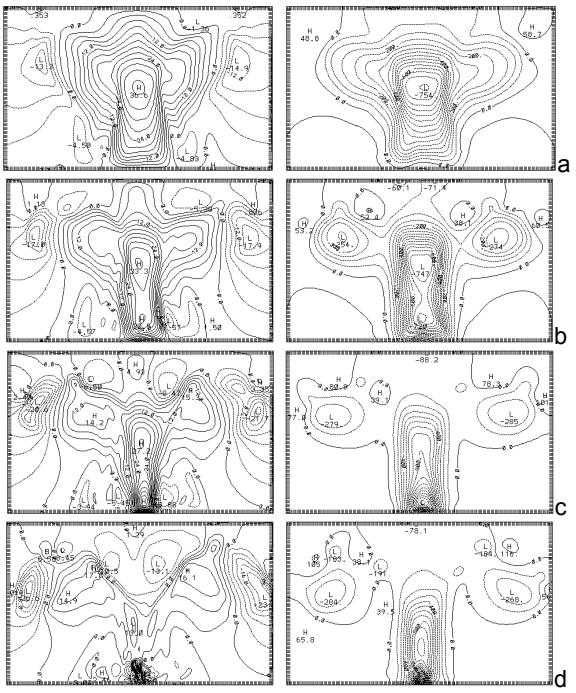

Fig. 4: Vertical motion w (left panels) and pressure perturbation p' (right panels) for CR at: 1860 s (a); 2160 s (b); 2310 s (c); and 2460 s (d). Units of w are m s-1. Units of p' are Pa. Contour intervals are w = 4 m s-1; p' = 50 Pa in a and b, and 100 Pa in c and d.

Starting at 2490 s, an axial downdraft proceeds from the top of the storm through the updraft owing to the downward directed vertical pressure gradient and causes the tornado to evolve into a two-celled structure before dissipating the tornado. Shortly afterwards, rain falling in to the weakened updraft collapses the entire storm. This sequence of events is close to those that proceed in Davies-Jones' (2008) experiment.

3.4.2 Stable layer experiments

ST2, ST3, ST4, and ST5 each produce tornado strength vortices, and mimic the mechanism of tornadogenesis by a descending rain curtain that was demonstrated in CR.

As low-level static stability increases, tornadogenesis is slightly delayed. Tornadogenesis occurs in CR at about 2310 s; 2370 s in ST2; 2400 s in ST3; 2400 s in ST4; and 2430 s in ST5. Also, tornado strength decreases as low-level static stability increases. Maximum values of ζ', -p', and w for the four experiments and CR are summarized in Table 5.

The tornadoes ingest potentially cold air from the stable layer, which decreases core buoyancy (example from ST5 in Fig. 5a). This is most apparent in the sharp decreases in the maximum pressure deficit among the experiments. As stability increases and the tornadoes ingest progressively colder air, upward velocities in the corner flow region expend energy to loft colder air, delaying tornadogenesis. They are also less able to sustain extreme pressure deficits that result in decreased tornado strength.

As hypothesized in Section I, the nature of inflow into the tornado does change with stable boundary layers. Potentially warm air is drawn from the dry neutral layer into the underlying stable layer along the lateral boundary of the tornado, and is circulated into the tornado (Fig. 5a).

	Max{ζ'} (s^{-1})	Max{-p'} (Pa)	Max{w} (m s^{-1})
CR	1.37	11216.5	131.7 (3.9)
ST2	1.30	10158.0	131.5 (3.9)
ST3	1.25	9513.9	128.7 (3.8)
ST4	1.10	8449.5	122.3 (3.6)
ST5	1.07	7892.6	117.1 (3.4)

Table 4: Maximum values of ζ', -p', and w in the tornado-like vortices. In paraentheses in the Max{w} column is the multiple by which the maximum wind speed exceeds the thermodynamic speed limit W_0.

Inflow into the tornado is maximized just above the stable layer and near the lower boundary of the overlying dry neutral layer (example from ST5 in Fig. 5b). This ranges from about one-half (ST1) to one kilometer (ST5) higher than the level of maximum inflow in CR, which is just above the surface.

5. SUMMARY AND CONCLUSIONS

Our climatology confirms the following results of other climatologies:

1. Geographic maximum in Gulf Coast states during the cool season
2. Preference for QLCS storm mode rather than isolated cells

We also found that over half of the cases with RUC-2 proximity soundings had shallow stable layers in at least one sounding before and/or after the tornado occurred. These findings indicate that it would be valuable to investigate the dynamics unique to QLCSs, in relation to tornadogenesis.

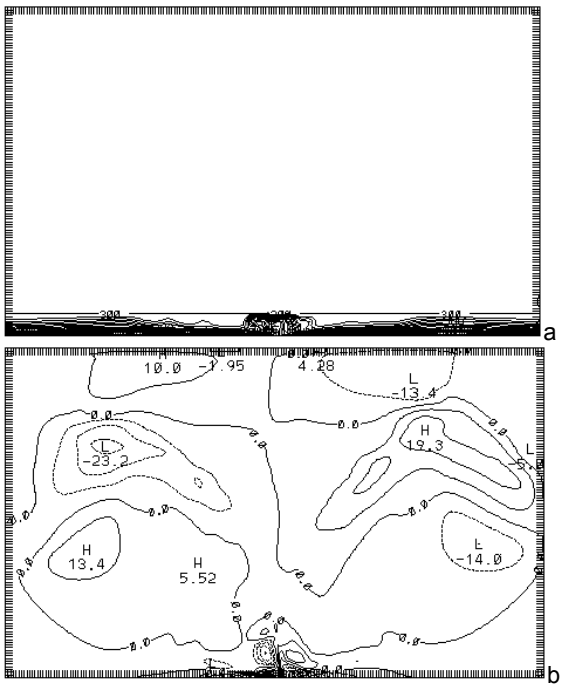

Fig. 5: Potential temperature (θ) contours (a) and u-component wind contours (b) at 2550 s in ST5. (Units of θ are K. Units of u are m s^{-1}. The contour interval of θ = 0.1 K; and the contour interval of u = 7 m s^{-1}.)

In our numerical modeling experiments, we demonstrated a mechanism of tornadogenesis that occurs independently of the mid-level mesocyclone, and low-level rotation is due solely to angular momentum transported to near the ground by hydrometeors. With this mechanism, tornadogenesis and strong tornado-like vortices are possible despite high static stability in the lowest kilometer. Tornadogenesis by the DPE was not possible in such stable layers in previous simulations by LS78. Thus, we have demonstrated a mechanism by which strong tornadoes may be possible in stable boundary layers. Our results suggest that changes in the geometry of inflow due to the presence of a shallow stable layer are possible.

6. REFERENCES

Ashley, W. S., 2007: Spatial and temporal analysis of tornado fatalities in the United States: 1880 – 2005. *Wea. Forecasting*, **22**, 1214 – 1228.

Davies-Jones, R., 2008: Can a Descending Rain Curtain in a Supercell Instigate Tornadogenesis Barotropically? *J. Atmos. Sci.*, **65**, 2469–2497.

Fiedler, B. H., and R. Rotunno, 1986: A theory for the maximum windspeed in tornado-like vortices. *J. Atmos. Sci.*, **43**, 2328–2340.

Fike, P. C., 1993: A climatology of nocturnal severe local storms outbreaks. Preprints, 17th Conf. on Severe Local Storms, St. Louis, MO, Amer. Meteor. Soc., 10-14.

Guyer, J.L., D.A. Imy, A. Kis, and K. Venable, 2006: Cool season significant (F2-F5) tornadoes in the Gulf Coast states. Preprints, 23nd Conf. Severe Local Storms, St. Louis MO, Amer. Meteor. Soc., CD-ROM

Hart, J. A., 1993: SVRPLOT: A new method of accessing and manipulating the NSSFC Severe Weather Database. Preprints, 17th Conf. on Severe Local Storms, St. Louis, MO, Amer. Meteor. Soc., 40-41.

Hart, J., and J. Korotky, 1991: The SHARP workstation v1.50, A skew-t/hodograph analysis and research program for the IBM and compatible PC, user's manual. National Weather Service, National Oceanic and Atmospheric Administration, U.S. Department of Commerce, 62 pp.

Klemp, J. B., and R. Wilhelmson, 1978: The simulation of three-dimensional convective storm dynamics. *J. Atmos. Sci.*, **35**, 1070-1096.

Leslie, L. M., 1971: The development of concentrated vortices: A numerical study. J. Fluid Mech., 48, 1–21.

Leslie, L. M., and R. K. Smith, 1978: The effect of vertical stability on tornadogenesis. J. Atmos. Sci., 35, 1281–1288.

Lewellen, D.C., and W.S. Lewellen, 2007: Near-Surface Intensification of Tornado Vortices. *J. Atmos. Sci.*, **64**, 2176–2194.

Trapp, R. J., S. A. Tessendorf, E. S. Godfrey, and H. E. Brooks, 2004: Tornadoes from squall lines and bow echoes. Part I: Climatological distribution. *Wea. Forecasting*, **20**, 23-34.